Bulletin of the Seismological Society of America. Vol. 59, No. 4, pp. 1569–1589. August, 1969

STRAIN ADJUSTMENTS ASSOCIATED WITH EARTHQUAKES IN SOUTHERN CALIFORNIA

By Stewart W. Smith and William Van de Lindt

ABSTRACT

A technique for the calculation of strain changes in a two-dimensional elastic body with arbitrary internal dislocations is presented. This technique is applied to the southern California region by assigning a specific fault and fault slip function for each major earthquake that has occurred since 1812. Although the model used has serious shortcomings when applied to the real Earth, certain important features concerning strain energy changes associated with earthquakes are brought out. The occurrence of earthquakes over the past 150 years has resulted in net increases in stored strain energy in a number of regions including the northern end of the Gulf of California, the Cajon Pass area, and the northern part of the Carizzo Plain. Large regions of strain energy decrease can also be seen, the most important of which is in the vicinity of Fort Tejon.

Introduction

The state of stress or strain in the Earth is the single most important property of the Earth that is pertinent to the occurrence of earthquakes. Despite the existence of faults on which activity has occurred in the past, no future earthquakes will be expected in a region unless some elastic strain has accumulated there. Currently there are four different means of measuring or inferring the state of stress in the Earth: direct observation of in-situ stress by means of stress relief measurements in bore holes and mines, geodetic measurements of crustal deformation, secular strain measurements by means of sensitive extensometers, and earthquake energy release measurements. Of these, only the last technique mentioned allows one to infer the properties of strain or strain change over a large region instead of at a single point where the observation is made. If the strain field of the Earth's crust is as complicated as one might guess from the complexity of near surface geologic structures in tectonically active areas, then single point measurements of stress will be difficult if not impossible to interpret. The prospects for such measurements on networks dense enough to give an areal view of the strain field are not encouraging due to the difficulty and expense of individual measurements.

If, as clearly seems to be the case, earthquakes are viewed as rapid episodes of stress release along existing faults, it is possible to calculate the resulting strain change for a number of events in a region and, by summing the result, see the overall pattern of stress release associated with seismic activity. Benioff (1951) proposed such a technique in which earthquake magnitude is converted to strain energy release, and a volume is assumed for each source thus allowing the conversion of total energy release to equivalent strain release. This technique has been used extensively, and although shortcomings have been discussed by Tsuboi (1952), it is a useful means of displaying the past seismic history of a region. Its relation to actual elastic strain release is not clear. One shortcoming is that it is necessary to assign a value of strain release, calcu-

lated from the magnitude, to a single point on the Earth's surface. No account can be taken of the different volume undergoing release during a large earthquake as compared with a small one, nor can any geometrical effects related to the direction of faulting be considered. In this paper we propose a different means of calculating the strain release associated with earthquakes; further, the technique we use makes clear that each earthquake increases the strain energy density in some regions of the crust while decreasing it in others. Thus the objective becomes the display of patterns of strain release and accumulation due to the occurrence of earthquakes.

Model

The model we use to represent earthquake occurrences is the generation of a stress-free plane surface within a pre-stressed elastic plate. The general problem of representing a seismic region such as California with a time varying stress, and with a sequence of stress-free cracks occurring at various times allowing slip, but subsequently locking, seems beyond our computational capability at the moment. We have posed the problem in a much simpler manner. The simplifications made detract somewhat from the pertinence of our model to the real Earth, so they will be discussed in some detail later. The problem is solved in two separate steps. First, during a specified interval of time all large earthquake occurrences are assigned to specific faults based on field evidence, macroseismic data, geologic inference, or guess work. Next, it is assumed that all such large earthquakes release a shear stress along their surface of approximately 50 bars. Under the assumption of plane strain, we can now calculate what the slip across the fault will be using a result of Starr (1928). This result is in rough accord with recent field evidence of slip variation along vertical strike-slip faults. Thus we have a set of discontinuities defined in our elastic plate, along which we have assigned specific slip functions. We now solve the static elastic problem of the deformation of this plate due to the presence of these discontinuities. In order to make the two problems consistent with one another, namely the problem of fault displacements and elastic deformation, we subject the elastic plate to a uniform shear stress of 50 bars, and we use the boundary condition that this stress remains constant on the boundaries while deformation is taking place on the internal discontinuities. To illustrate what this procedure accomplishes note that if we insert a single fault, along a straight line at 45° to the principal axis of stress, and use the slip function calculated from Starr (1928), the result of our numerical solution would show that the stress along this fault has dropped to zero. No direct interaction of faults can be considered with this technique, it is as if after each fault slips, it is locked and the stress field becomes homogenized before the next earthquake is permitted to occur. Nonetheless certain types of interactions can be seen. In the simple case of two separate sections of a fault slipping during two earthquakes, with an undisturbed section in between, this technique allows a quantitative measure of the strain accumulation on the middle section of the fault. As will be seen in later examples, regions of strain accumulation occur not only at the ends of the faults but also in broader regions in directions normal to the fault surface. In regions where there are numerous parallel branches of active faults, this technique allows the superposition of these regions of strain accumulation producing hitherto unsuspected regions of possible high stress. If a section of a fault is known to be undergoing slow creep, the creep displacement function can be entered along with the earthquake fault displacements to obtain the net elastic deformation of the region. No such data was used in this particular study however.

For the larger earthquakes in California, which dominate the stress release picture, we believe the plane strain model is a reasonable approximation for the description of the deformation that occurs. It seems particularly appropriate if the San Andreas fault is viewed as a transform fault and the crust as an elastic plate moving over a plastic zone in the upper mantle. In this case one would expect stress to have been released through the entire thickness of the crust after the occurrence of an earthquake.

Analysis

The two-dimensional case of plane strain (or stress) can be solved with the help of the Airy stress function (Fung, 1965). This function satisfies the biharmonic equation

$$\nabla^4\phi = 0 \tag{1}$$

except in points where slippage has taken place. In these points where the displacement is two-valued and the compatibility conditions are not satisfied, special conditions will be required.

It is possible of course to formulate the entire problem in terms of dislocation theory, that is by calculating the appropriate Green's function and using it along with the specified slip along internal boundaries to generate the solution everywhere (Chinnery, 1963). However, since the eventual solution to our problem must be numerical because of the irregular boundaries, we chose to formulate the problem as a differential equation the solution of which can be obtained by an iterative technique. The stresses are obtained from the function ϕ as follows:

$$\begin{aligned} \sigma_{xx} &= \frac{\partial^2\phi}{\partial y^2} \\ \sigma_{yy} &= \frac{\partial^2\phi}{\partial x^2} \\ \sigma_{xy} &= -\frac{\partial^2\phi}{\partial x \partial y}. \end{aligned} \tag{2}$$

On the outside boundary of a two-dimensional region the traction T is given in direction and magnitude. It can be expressed in terms of the function ϕ by

$$\begin{aligned} T_x &= \cos\theta \frac{\partial^2\phi}{\partial y^2} - \sin\theta \frac{\partial^2\phi}{\partial x \partial y} \\ T_y &= -\cos\theta \frac{\partial^2\phi}{\partial x \partial y} + \sin\theta \frac{\partial^2\phi}{\partial x^2}. \end{aligned} \tag{3}$$

In these equations θ is the angle between the outward directed normal on the boundary and the X-axis of the coordinate system. These equations can be obtained immediately from Figure 1 by considering the equilibrium of a small triangular region.

From Figure 2 it can be seen that $\sin\theta = -dx/ds$ and $\cos\theta = dy/ds$. Substituting this in equation (3) gives

$$\begin{aligned} T_x &= \frac{\partial^2\phi}{\partial y^2}\frac{dy}{ds} + \frac{\partial^2\phi}{\partial x \partial y}\frac{dx}{ds} = \frac{d}{ds}\left(\frac{\partial\phi}{\partial y}\right) \\ -T_y &= \frac{\partial^2\phi}{\partial x \partial y}\frac{dy}{ds} + \frac{\partial^2\phi}{\partial x^2}\frac{dx}{ds} = +\frac{d}{ds}\left(\frac{\partial\phi}{\partial x}\right). \end{aligned} \tag{4}$$

The problem described in this paper is solved in a rectangular region. Furthermore it is assumed that T_x is a constant and $T_y = 0$ on the sides parallel to the Y-axis. On the other two sides $T_x = 0$ while T_y is equal to a constant. The constants are equal and have opposite signs. The planes of maximum shear are the planes under 45° with the coordinate axes. Figure 3 shows the assumed forces and maximum shear planes. The arrows alongside those planes indicate the relative motion that would take place if a cut in the rectangle were made, parallel to the planes of maximum shear stress.

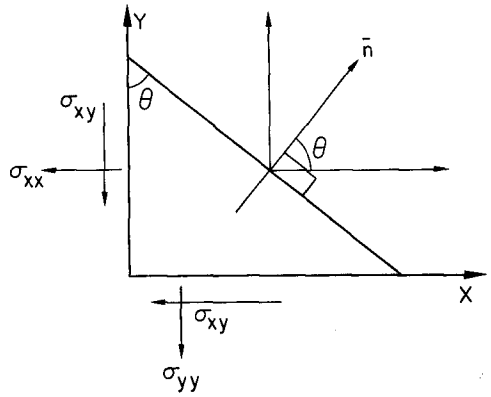

FIG. 1. Traction on the outside boundary of a two dimensional region.

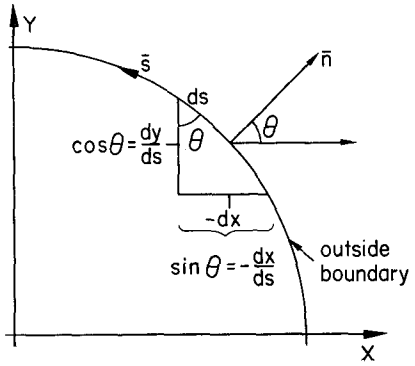

FIG. 2. Boundary conditions on the outside of the region.

In the case of a rectangle the conditions (4) can be simplified as follows. For instance, considering the side of the rectangle coinciding with the X-axis, integration of T_x in equation (4) gives

$$\int_0^x T_x\, ds = \int_0^x \frac{d}{ds}\left(\frac{\partial \phi}{\partial y}\right) ds = \left(\frac{\partial \phi}{\partial x}\right)_x - \left(\frac{\partial \phi}{\partial y}\right)_0 = C$$

if the value $T_x = 0$ is used, as given in Figure 3. The value of the constant C is usually chosen to be equal to zero. This assures continuity of $\partial\phi/\partial n$ and therefore faster convergence of iterative methods of solution.

Furthermore T_y can be integrated twice resulting in

$$\int_0^x dx \int_0^x \frac{d}{ds}\left(\frac{\partial \phi}{\partial x}\right) ds = \phi(x) - \phi(0) = \frac{-\sigma}{} x^2 + c_3 x + c_2.$$

The constants c_2 and c_3 are constants of integration and can be chosen so that the function ϕ is continuous in the corners of the rectangle.

Similar integrations can be performed on the other three sides of the rectangle. If the values of ϕ and $\partial\phi/\partial n$ are matched in the corners, the resulting functions for ϕ and $\partial\phi/\partial n$ on the boundary are as given in Figure 4. In these expressions the constants c_1, c_2 and c_3 can be chosen arbitrarily, however c_4 and c_6 depend on c_1, c_2 and c_3. This dependency is given in the same figure.

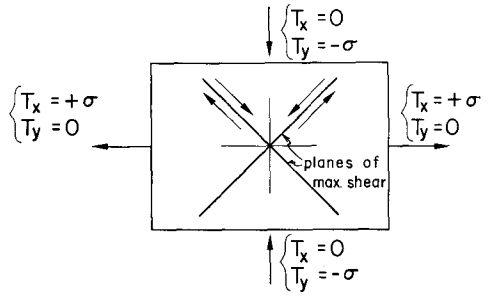

FIG. 3. Boundary stresses used for a rectangular region.

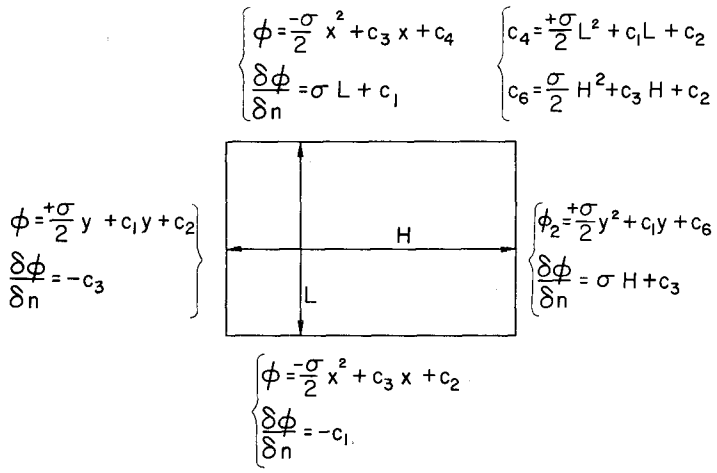

FIG. 4. The values of ϕ that result using constant stress on the boundary and matching the values of ϕ in the corners.

Conditions at a fault. An earthquake is modeled here as a slip along an, in general, curved line. The amount of slippage as a function of position along the fault is, as previously discussed, assumed to be known. This condition can be stated as

$$u_1(s) = u_2(s) + f_x(s)$$

$$v_1(s) = v_2(s) + f_y(s) \tag{5}$$

where s is the coordinate along the fault curve, u_1 and u_2 are the absolute displacements along the fault in X direction and v_1 and v_2 are those in Y direction. $f_x(s)$ and $f_y(s)$ are the given slip along the fault in the x and y directions.

There are two more conditions that must be met, the normal stress and the tangential stress must be continuous across the fault boundary. If curvilinear coordinates are used, as shown in Figure 5, these two conditions result in

$$(\sigma_{nn})_{\mathrm{I}} = \left(\frac{\partial^2\phi}{\partial s^2} - \frac{1}{\rho}\frac{\partial\phi}{\partial n}\right)_{\mathrm{I}} = \left(\frac{\partial^2\phi}{\partial s^2} - \frac{1}{\rho}\frac{\partial\phi}{\partial n}\right)_{\mathrm{II}} = (\sigma_{nn})_{\mathrm{II}} \tag{6a}$$

$$(\sigma_{sn})_{\mathrm{I}} = \left(\frac{\partial^2\phi}{\partial s\partial n}\right)_{\mathrm{I}} = \left(\frac{\partial^2\phi}{\partial s\partial n}\right)_{\mathrm{II}} = (\sigma_{sn})_{\mathrm{II}}. \tag{6b}$$

Remaining now is the problem of expressing the conditions (5) by means of the function ϕ and its derivatives. This can be done by slightly extending a method described by Zienkiewicz and Gerstner (1959). First a rigid rotation is added to equations (5a and 5b)

$$u_1 = u_2 + \alpha y + \beta + f_x(s) \tag{7a}$$

$$v_1 = v_2 - \alpha x + \delta + f_y(s). \tag{7b}$$

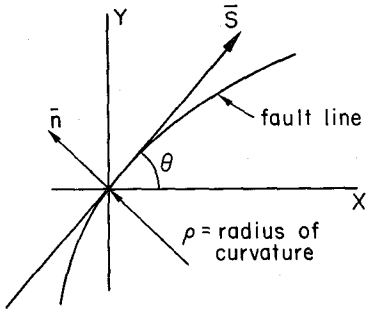

FIG. 5. Curvilinear coordinates used on a fault.

This does not alter the stresses or strains as can be verified by calculating $\partial u/\partial x$, $\partial v/\partial y$ and $\partial u/\partial y + \partial v/\partial x$.

Differentiating with respect to s, the curvilinear coordinate, and eliminating α from the resulting equations, gives

$$\cos\theta\frac{\partial u_1}{\partial s} + \sin\theta\frac{\partial v_1}{\partial s} = \cos\theta\frac{\partial u_2}{\partial s} + \sin\theta\frac{\partial v_2}{\partial s} + \cos\theta\frac{\partial f_x}{\partial s} + \sin\theta\frac{\partial f_y}{\partial s}. \tag{8}$$

The slip function f_x and f_y are now transformed into f_s and f_n, the tangential and normal displacement on the fault. This is accomplished with the help of

$$f_x = f_s\cos\theta - f_n\sin\theta$$

$$f_y = f_s\sin\theta + f_n\cos\theta$$

from which it follows that

$$\cos\theta\frac{\partial f_x}{\partial s} + \sin\theta\frac{\partial f_y}{\partial s} = \frac{\partial f_s}{\partial s} - \frac{f_n}{\rho}. \tag{9}$$

Use is made of the relation $1/\rho = \partial\theta/\partial s$ in which ρ is the radius of curvature of the fault line.
Furthermore,

$$\frac{\partial u}{\partial s} = \frac{\partial u}{\partial x}\cos\theta + \frac{\partial u}{\partial y}\sin\theta \tag{10a}$$

$$\frac{\partial v}{\partial s} = \frac{\partial v}{\partial x}\cos\theta + \frac{\partial v}{\partial y}\sin\theta. \tag{10b}$$

Substituting equations (9, 10a and 10b) into equation (6) gives

$$\frac{\partial u_1}{\partial x}\cos^2\theta + \frac{\partial v_1}{\partial y}\sin^2\theta + \left(\frac{\partial u_1}{\partial y} + \frac{\partial v_1}{\partial x}\right)\sin\theta\cos\theta = \frac{\partial u_2}{\partial x}\cos^2\theta + \frac{\partial v_2}{\partial y}\sin^2\theta + \left(\frac{\partial u_2}{\partial y} + \frac{\partial v_2}{\partial x}\right)\sin\theta\cos\theta + \frac{\partial f_s}{\partial s} - \frac{f_n}{\rho}. \tag{11}$$

The equations of elasticity can be written as

$$e_{xx} = \frac{\partial u}{\partial x} = A\left(\frac{\partial^2\phi}{\partial y^2} - B\frac{\partial^2\phi}{\partial x^2}\right)$$

$$e_{yy} = \frac{\partial v}{\partial y} = A\left(\frac{\partial^2\phi}{\partial x^2} - B\frac{\partial^2\phi}{\partial y^2}\right)$$

$$e_{xy} = \left(\frac{\partial u}{\partial y} + \frac{\partial v}{\partial x}\right) = -2A(1 + B)\frac{\partial^2\phi}{\partial x\partial y} \tag{12}$$

where, for the plane strain case $1/A = E/(1 - \nu^2)$ and $B = \nu/(1 - \nu)$. E is the modulus of elasticity, ν is Poisson's ratio. Equation (12) is substituted in equation (11) and the resulting equation is transformed from the coordinates X and Y to the curvilinear coordinates s and n. The following result is obtained:

$$A_1\left\{\frac{\partial^2\phi}{\partial n^2} - B_1\left(\frac{\partial^2\phi}{\partial s^2} - \frac{1}{\rho}\frac{\partial\phi}{\partial n}\right)\right\}_{\text{I}} = A_2\left\{\frac{\partial^2\phi}{\partial n^2} - B_2\left(\frac{\partial^2\phi}{\partial s^2} - \frac{1}{\rho}\frac{\partial\phi}{\partial n}\right)\right\}_{\text{II}} + \frac{\partial f_s}{\partial s} - \frac{f_n}{\rho} \tag{13}$$

In this equation A_1 and B_1 refer to the elastic constants of the material on the outside of the fault, A_2 and B_2 to those on the inside. Outside and inside are determined by the normal on the fault which points from material with index 2 to that with index 1. The normal points from inside to outside.

Equation (13) can be simplified if $A_1 = A_2$ and $B_1 = B_2$. In that case, because of equation (6a)

$$\left(\frac{\partial^2\phi}{\partial n^2}\right)_{\text{I}} = \left(\frac{\partial^2\phi}{\partial n^2}\right)_{\text{II}} + \frac{1}{A}\left(\frac{\partial f_s}{\partial s} - \frac{f_n}{\rho}\right). \tag{14}$$

This is the first interface condition which results from the discontinuity across the fault surface specified by equation (5a) and (5b). One more condition can be obtained

as follows. Differentiating equations (7a and 7b) twice and eliminating α gives

$$\cos\theta\frac{\partial^2 v_1}{\partial s^2}-\sin\theta\frac{\partial^2 u_1}{\partial s^2}=\cos\theta\frac{\partial^2 v_2}{\partial s^2}-\sin\theta\frac{\partial^2 u_2}{\partial s^2}+\cos\theta\frac{\partial^2 f_y}{\partial s^2}-\sin\theta\frac{\partial^2 f_x}{\partial s^2}. \quad (15)$$

First the dependent variables f_x and f_y are transformed into f_s and f_n as was done before. This gives:

$$\cos\theta\frac{\partial^2 f_y}{\partial s^2}-\sin\theta\frac{\partial^2 f_x}{\partial s^2}=\frac{\partial^2 f_n}{\partial s^2}+\frac{2}{\rho}\frac{\partial f_s}{\partial s}+f_s\frac{\partial}{\partial s}\left(\frac{1}{\rho}\right)-\frac{f_n}{\rho^2}. \quad (16)$$

Next the independent variable s is transformed into X and Y. Substituting equation (12) results in

$$-A_1\left\{\frac{\partial}{\partial n}(\nabla^2\phi)_{\mathrm{I}}+(1+B_1)\frac{\partial}{\partial s}\left(\frac{\partial^2\phi}{\partial s\partial n}\right)\right\}_{\mathrm{I}}=-A_2\left\{\frac{\partial}{\partial n}(\nabla^2\phi)_{\mathrm{II}}\right.$$

$$\left.+(1+B_2)\frac{\partial}{\partial s}\left(\frac{\partial^2\phi}{\partial s\partial n}\right)\right\}_{\mathrm{II}}+\frac{\partial^2 f_n}{\partial s^2}+\frac{2}{\rho}\frac{\partial f_s}{\partial s}+f_s\frac{\partial}{\partial s}\left(\frac{1}{\rho}\right)-\frac{f_n}{\rho^2}. \quad (17)$$

Again if both constants A and B are the same on each side of the fault equation (17) simplifies to

$$\frac{\partial}{\partial n}(\nabla^2\phi)_{\mathrm{I}}=\frac{\partial}{\partial n}(\nabla^2\phi)_{\mathrm{II}}-\frac{1}{A}\left(\frac{\partial^2 f_n}{\partial s^2}+\frac{2}{\rho}\frac{\partial f_s}{\partial s}+f_s\frac{\partial}{\partial s}\left(\frac{1}{\rho}\right)-\frac{f_n}{\rho^2}\right). \quad (18)$$

This follows immediately from using equation (6b).

Before proceeding to the final form of these equations, it will be necessary to change equations (6a and 6b) to their final form. Integrating equation (6b) with respect to s gives

$$\left(\frac{\partial\phi}{\partial n}\right)_{\mathrm{I}}=\left(\frac{\partial\phi}{\partial n}\right)_{\mathrm{II}} \quad (19)$$

since at both ends of the fault $\partial\phi/\partial n$ is continuous. Using equation (19) and integrating equation (6a) twice gives

$$(\phi)_{\mathrm{I}}=(\phi)_{\mathrm{II}} \quad (20)$$

at every point along the fault, again using the conditions that off the ends of the fault in the undisturbed region ϕ is single valued and is continuous.

For the numerical method used it is easier to use as a condition on the fault, the sum of equation (6a) and equation (14), rather than equation (14) itself. This gives:

$$(\nabla^2\phi)_{\mathrm{I}}=(\nabla^2\phi)_{\mathrm{II}}+\frac{1}{A}\left(\frac{\partial f_s}{\partial s}-\frac{f_n}{\rho}\right)$$

as

$$\nabla^2\phi=\frac{\partial^2\phi}{\partial n^2}+\frac{\partial^2\phi}{\partial s^2}-\frac{1}{\rho}\frac{\partial\phi}{\partial n} \quad (21)$$

Conditions (18) and (21) can be simplified further if it is assumed that the radius of curvature of the fault is so large that all terms involving ρ in equations (18) and (21) can be neglected. It will further be assumed that the fault does not open up so that $f_n = 0$. This will actually be the case if the faulting occurs in a pure shear stress field and the displacements are small (Starr, 1928). Under those conditions equations (18) and (21) become:

$$(\nabla^2\phi)_{\mathrm{I}} = (\nabla^2\phi)_{\mathrm{II}} + \frac{1}{A}\frac{\partial f_s}{\partial s} \tag{22}$$

$$\left(\frac{\partial}{\partial n}\nabla^2\phi\right)_{\mathrm{I}} = \left(\frac{\partial}{\partial n}\nabla^2\phi\right)_{\mathrm{II}}. \tag{23}$$

Equations (19), (20), (22) and (23) are the conditions to be satisfied on a fault.

Behavior of f_s along a fault. The problem as stated above can be solved provided f_s is known. As discussed earlier we use some of the analytic results of Starr (1928) who treated the case of a crack in a plate, assuming a uniform shear stress at infinity. From his paper it can be seen that

$$f_s = -\frac{3}{2}\frac{Sc}{\mu}\sqrt{1-(x/c)^2} \tag{24}$$

in which S is the shear stress, c is the half length of the fault and μ is Lame's constant. As $\mu = E/2(1+\nu)$ and using the approximation $\nu = \frac{1}{4}$

$$\frac{1}{A}\frac{\partial f_s}{\partial s} = 4S\frac{x/c}{\sqrt{1-(x/c)^2}}. \tag{25}$$

In the numerical calculation $4S$ is chosen to be equal to one, giving

$$\frac{1}{A}\frac{\partial f_s}{\partial s} = \frac{x/c}{\sqrt{1-(x/c)^2}}. \tag{26}$$

In order to relate the results of the calculation to the actual stresses in the crust, a scale factor must be used. Using an average value of $\frac{f_{\max}}{c}$ obtained from the data of King and Knopoff (1968) and substituting this in equation (24) gives an $S = 13$ bars. Other three dimensional approaches suggest a higher value. We have used a value of $S = 50$ bars in our calculations. If another value of S is desired the energy contour interval should be scaled by a factor $\left(\frac{S}{50}\right)^2$. The general shape of the contours is not affected by a change in the value of S. Fault lengths used for specific earthquakes are listed in Table 1 and were obtained from field evidence, macroseismic data, or from a magnitude fault length relation. The relation we used is $L = 10^{.59M-2.24}$ km which fits California earthquakes in the magnitude range 6.0–8.2. If equation (26) is used it is assumed that the stress S is constant along the fault and that complete stress release on the fault is obtained. Neither condition is completely fulfilled in practice, however it was considered a reasonable first approximation. Friction on the fault, for instance, causes the stress to be released only partially and the stress S will vary along the fault.

Numerical Method

The problem as stated above was solved numerically on a digital computer. As is usual in the case of solving partial differential equations, the domain of integration is covered with two sets of vertical and horizontal, parallel lines, neither of which need be equidistant. The faults are approximated by line segments passing through the grid points, the points of intersection of the two sets of lines. An example is given in Figure 6.

TABLE 1

Large Earthquakes in Southern California Region 1812-1966

Event No.	Date	Magnitude	Locality	Equivalent Fault Length in km
1	1812	7.8+ (outstanding)	Santa Barbara Channel	80
2	1857	7.8+ (outstanding)	Fort Tejon	250
3	1892	7+ (great)	Agua Blanca	100
4	1899	7+ (great)	San Jacinto	100
5	1903	7+ (great)	Colorado Delta	100
6	1915	6.2	Calexico	29
7	1915	7.1	Colorado Delta	87
8	1916	6.0	Tejon Pass	20
9	1918	6.8	San Jacinto	58
10	1923	6.2	Riverside	29
11	1925	6.3	Santa Barbara	30
12	1933	6.3	Long Beach	30*
13	1934	6.5	Colorado Delta	40
14	1934	7.1	Colorado Delta	87
15	1935	6.0	Colorado Delta	20
16	1937	6.0	Terwilliger Valley	20
17	1940	7.1	Imperial Valley	87
18	1941	6.0	Colorado Delta	20
19	1941	6.0	Santa Barbara	20
20	1942	6.5	Borrego Valley	40
21	1946	6.3	Walker Pass	30
22	1947	6.4	Manix	34
23	1948	6.5	Desert Hot Springs	18*
24	1952	7.7	Tehachapi	70*
25	1952	6.1	Tehachapi	23
26	1952	6.1	Tehachapi	23
27	1954	6.2	Santa Rosa Mtn	28
28	1954	6.3	Agua Blanca	30
29	1956	6.8	San Miguel	58
30	1956	6.4	San Miguel	34
31	1966	6.3	Gulf of California	40*

* Length of aftershock region.

Next the location of the fault line must be given. This can be done in several ways, however because of the method of solution of the differential equation (point iteration) the following method was adopted. A set of code words is given as input with format

$$a \quad b$$

This is to be read as: apply finite difference operator "a" in the next "b" points. After this "b" values of $(1/A)(\partial f_s/\partial s)$ are given. The finite difference operator can be one of several, for instance, it can be the finite difference approximation of the operator ∇^4 or

it could be a special operator used at the internal dislocations. All points inside the rectangular domain are described this way, horizontal line after horizontal line. For instance, the fifth line in Figure 6 is described as:

$$\begin{array}{lll} 21 & & 3 \\ 15 & & 1 \\ \dfrac{1}{A} & \dfrac{\partial f_s}{\partial s} & \\ 21 & & 2 \end{array}$$

Points on the boundaries are deleted. The above code words read: Do three points with operator 21 (which is the finite difference approximation of ∇^4) then do one point with operator 15 (which is one of twenty interface operators used on the fault lines). The value of $(1/A)(\partial f_s/\partial s)$ must be given next. The last code word for this line reads:

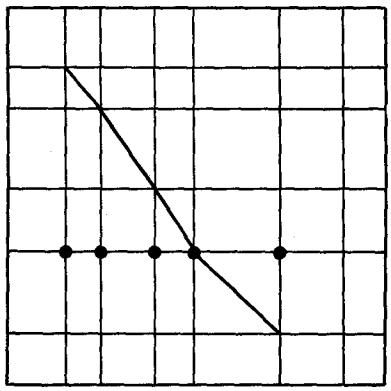

FIG. 6. A section of the grid used illustrating the representation of an arbitrary fault.

Do two points with operator 21. As an example, a derivation of one particular operator for use on an irregular boundary is given in the Appendix.

Point relaxation was used to solve the equations resulting from discretizing the partial differential equation (1), together with the boundary and interface conditions. In order to simplify the finite difference expressions, especially those for points on the interfaces and points adjacent to the fault lines, the differential operator is split into:

$$\nabla^4\phi = \nabla^2(\nabla^2\phi) = 0$$

which can be written as:

$$\nabla^2 g = 0 \tag{28}$$

where

$$\nabla^2\phi = g. \tag{29}$$

These equations were solved as follows. A first guess of ϕ was made in all interior points

of the grid, the boundary values of ϕ being given. With the help of these values, g was calculated at each point of the grid using

$$g = L(\phi)$$

where L is the finite difference approximation to the differential operator ∇^2. For points

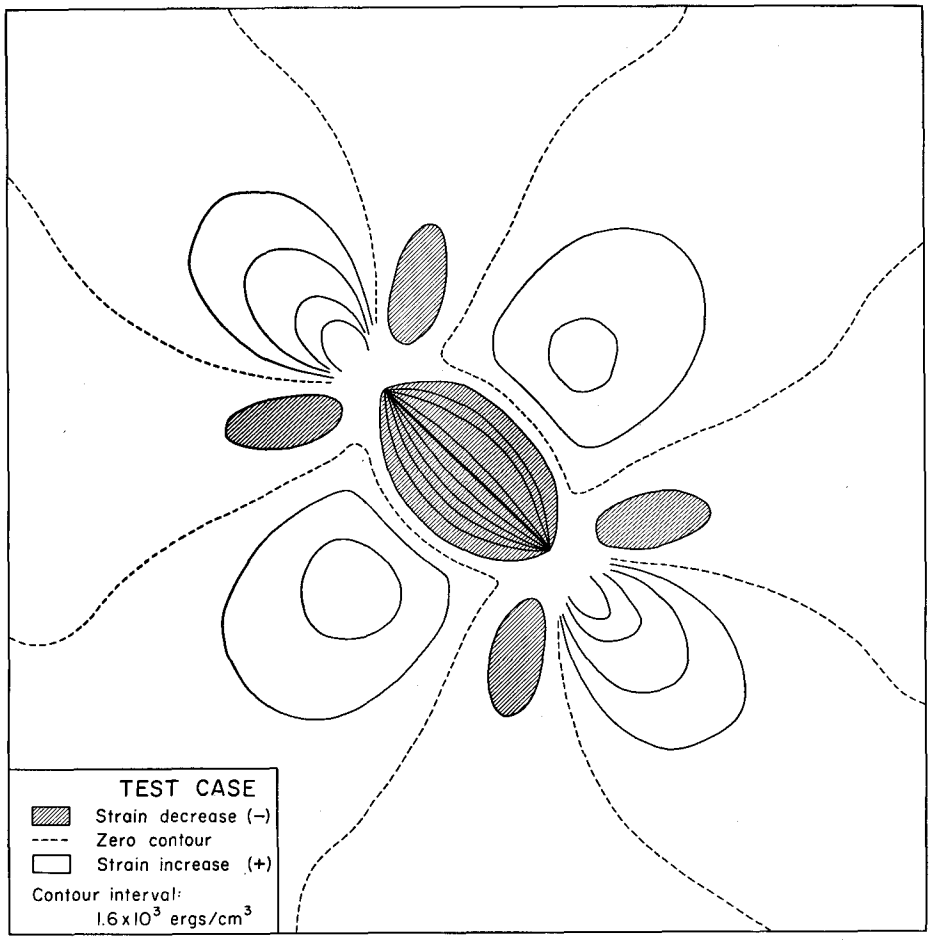

FIG. 7. Test case of a straight crack along plane of maximum shear. Calculated shear stress is zero along crack.

on the external boundaries use was made of the known value of $\partial\phi/\partial n$. For points on the fault lines special expressions were used, taking into account the discontinuity in g as given by equation (22). After this, all interior values of g are corrected by an iteration procedure with the help of equation (28). Then ϕ in the interior points is corrected by a similar iteration process, using equation (29). This whole process is repeated until the corrections in ϕ become small and a sufficiently accurate solution is obtained.

Yield Function. After the values of ϕ in the grid points are found, the stresses in each point can be calculated with the help of equation (2) and by numeric differentiation of the function ϕ. These stresses could be plotted as a function of position in the form of

contour maps, however most of the information needed is contained in the von Mises yield function. This function is simply that part of the elastic energy that depends on the asymmetrical part of the stress. It is given by Jeffreys (1962)

$$F = \tfrac{1}{3}\{(\sigma_{xx} - \sigma_{yy})^2 + (\sigma_{yy} - \sigma_{zz})^2 + (\sigma_{zz} - \sigma_{xx})^2 + 6\sigma_{xy}^2 + 6\sigma_{xz}^2 + 6\sigma_{yz}^2\}.$$

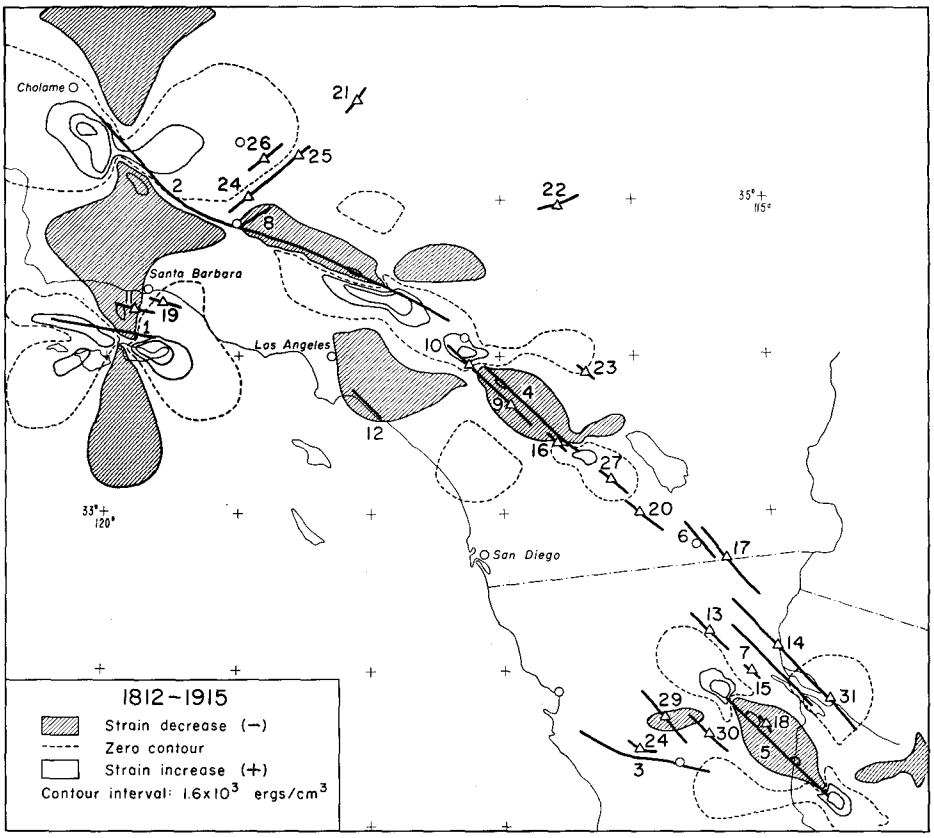

FIG. 8. Strain energy changes due to earthquakes in the interval 1812–1915. Triangles are instrumentally determined epicenters. Solid lines are inferred faults. Numbers are keyed to table of earthquakes.

For plane strain

$$\sigma_{zz} = \tfrac{1}{4}(\sigma_{xx} + \sigma_{yy})$$

$$\sigma_{yz} = \sigma_{xz} = 0$$

which gives:

$$F = \tfrac{1}{24}\{13\sigma_{xx}^2 + 13\sigma_{yy}^2 - 22\sigma_{xx}\sigma_{yy} + 48\sigma_{xy}^2\}.$$

This is the computed function which is displayed as contour plots in Figures 7–10. It is chosen as a convenient scalar field most closely related to the possible shear failure of the material and thus in our opinion closely related to the occurrence of earthquakes.

Discussion

In viewing the three strain maps, Figures 8, 9, 10, and comparing them with the strain release maps published by Allen *et al.* (1965) the most striking feature is the elongation of anomalies along existing faults as compared with the more diffuse patterns that resulted from earlier studies. This is to be expected of course, because the fault orientations and lengths are part of the input data in our analysis. It should also be recognized that considerable smoothing must be done to a conventional strain re-

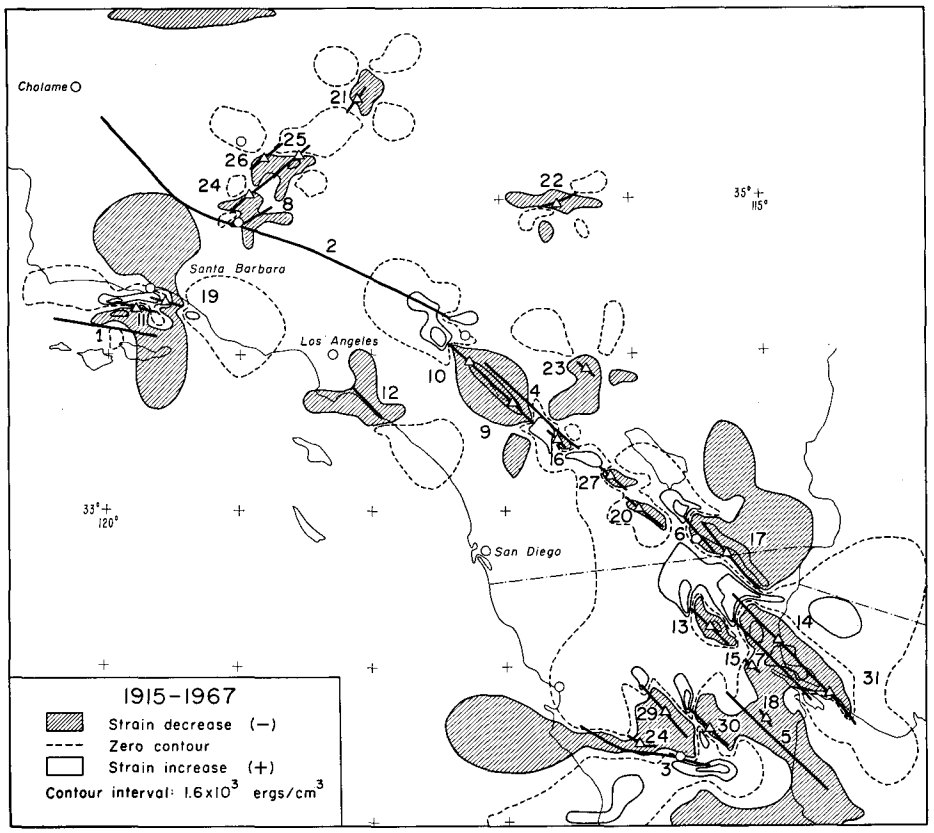

Fig. 9. Strain energy changes due to earthquakes in the interval 1915–1967. Triangles are instrumentally determined epicenters. Solid lines are inferred faults. Numbers are keyed to table of earthquakes.

lease display such as used by Benioff (1951) before it can be contoured. Since the basic data for the two representations is almost identical, one could view the approach we have used as the development of smoothing operators that are based on static elasticity theory, with additional data in the form of fault orientation and length, whereas in Benioff's case the operators simply smooth out the strain release uniformly in all directions. In addition, with our approach we now need to consider the significance of those regions whose strain energy density appears to have increased as a result of slip of nearby faults. There are of course a number of unanswered questions regarding this phenomenon. In a homogeneous elastic plate, once started, a crack on which the stress is concentrated near the end, as it is in Starr's case, would continue to propagate. One would have to apply other stresses, or assume some type of inhomogeneity in order to

explain why the crack actually stops propagating at some specific length. In actual earthquake occurrences there is some evidence that stress is concentrated near the ends of the active fault break as can sometimes be seen in the distribution of aftershocks. The crust is not homogeneous, the stress is not uniform, and the fault when it occurs is not a stress free surface but one on which slip is controlled by friction. With all of these inadequacies, we nevertheless proceed to make the calculation of strain changes due to earthquakes, with the belief that the result is closer to representing what actually occurs in the Earth than has previously been obtained.

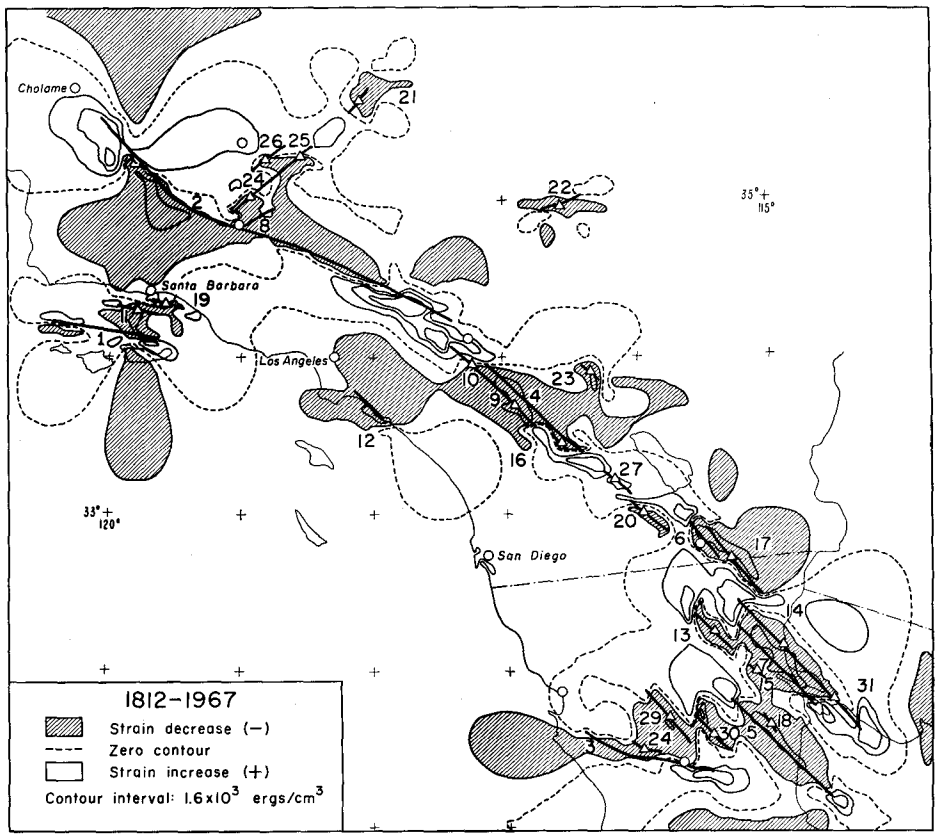

FIG. 10. Strain energy changes due to earthquakes in the interval 1812–1967. Triangles are instrumentally determined epicenters. Solid lines are inferred faults. Numbers are keyed to table of earthquakes.

A second point concerns total energy for the plate. Using the model as described one can see that the integrated energy over the plate due to the insertion of a stress free crack will tend to increase, whereas in the crust of the Earth, certainly the net result of an earthquake is to convert elastic strain energy into mechanical work and heat. Our result is entirely due to the constant stress boundary condition we have imposed; in fact the total energy change is almost completely arbitrary depending on the behavior at the boundaries far removed from the faults with which we are concerned. Saint Venant's principle however tells us that the patterns of strain release and accumulation we calculate for the interior of the plate cannot be seriously affected by stress variations on the boundary if it is far removed. Therefore we calculate and plot strain energy

density variations as a result of earthquake occurrences, but we do not calculate the integrated energy change for the entire plate.

As can be seen in the test case presented in Figure 7, there are four regions of stress concentration and five of stress release associated with each strike-slip fault. If the assumptions made in this approach are valid, then it would seem that the probabilities for earthquake occurrences are enhanced in those regions showing a stress concentration, as a direct result of the occurrence of a nearby earthquake. In order to test this hypothesis, the seismic history of southern California and Baja California was subdivided into two intervals, 1812–1915, and 1915–1966. All historic shocks after 1812 classified as "outstanding" by Wood and Heck (1951) are included as well as all shocks classified as "great" with the exception of the 1769 earthquake near Los Angeles. Great difficulty was experienced in relating some of these early events to specific faults, and it is recognized that this is a serious limitation of the strain maps presented here. In the interval following 1912, all earthquakes with magnitudes greater than 6 were included. The earthquakes used, and the appropriate fault lengths are given in Table 1 along with index numbers that key them to the strain maps. The basic data on earthquake occurrences and faulting was obtained from Richter (1958), and Allen *et al.* (1965). Along the San Andreas system there is little difficulty with the direction of faulting, and the inferred lengths cannot be far wrong as we can see by comparison with more recent events. In the Santa Barbara Channel, the direction of faulting is inferred to be parallel to the major transverse features exposed on land here. The length of the 1812 fault rupture in this area is assumed to be less than one would expect from an "outstanding" earthquake because of the likelihood that it had a significant component of dip slip motion. There is also a question, Richter and Nordquist (1958), concerning the direction of faulting and the aftershock distribution of the Manix earthquake. With these limitations in mind we must point out that the maps presented here cannot be used in detail to specify regions of high stress. In addition to the uncertainty of the faulting associated with historic earthquakes, and the inadequacies of the model discussed above, other mechanisms of stress release are undoubtedly acting which are not accounted for here and which could release the stress which apparently results from the fault slippage we have postulated. With that disclaimer, we now may examine the maps to see what geologic interpretations can be made.

Interpretation

In addition to the obvious strain accumulation-release pattern along the San Andreas fault, the 1915–1967 map (Figure 9) shows several features conjugate to this trend. The most striking of these is that formed by earthquakes in the Santa Barbara, Tehachapi, and Walker Pass regions. Ryall *et al.* (1966) using more conventional representations of seismic activity commented on this same trend and referred to it as the Ventura-Winnamucca zone. Benioff (1955) concluded that the 1952 earthquakes on the White Wolf fault were a mechanism for relief of localized stress on the curved section of the San Andreas fault near Fort Tejon. In the present paper we agree with this view and can see that although the aftershock distribution of the 1952 earthquakes did not extend to the San Andreas fault, the zone of strain release most certainly did. In addition we note that other earthquakes in the aforementioned band of conjugate activity may also have contributed to stress release here. Further to the southeast toward San Bernardino we see that earthquakes during the same time interval have resulted in a net increase in strain energy. When the next large earthquake occurs on this

section of the San Andreas fault, between San Bernardino and Fort Tejon, the fact that the strain field has been partially released near Fort Tejon will undoubtedly have an effect in determining the total length over which the fault will rupture, and will thus affect the maximum magnitude earthquake that can be expected here. Whether enough strain has been released to actually prevent a rupture from propagating past the bend at Fort Tejon cannot be determined from the data presented here.

The strain pattern on the San Andreas from San Bernardino to the Mexican border appears very narrow wth many shocks in excess of magnitude 6 distributed more or less uniformly along the zone. The recent earthquake near Borrego Mountain (April 9, 1968 Magnitude 6.4) is not included in the map; however it would not appreciably affect the existing pattern as described above. In Mexico, the pattern changes significantly with a broad area of stress release extending from the Colorado Delta to the Pacific Ocean. Also notable in this region is a significant area of strain energy increase east of the Colorado River. The increase here is the result of superposition of the effects of numerous parallel breaks at the head of the Gulf of Calfornia. The inference here, remembering all previous disclaimers, is that additional parallel breaks can be expected to further broaden this zone of stress release as this region of stress concentration undergoes relaxation in the future. The area investigated extends only about 100 km south of the border, so we cannot make any observations related to the presence of the East Pacific Rise and the possible offsets of the San Andreas system in the Gulf of California. It is clear however, that a major change in the strain field occurs near the southern boundary of our region near 32° North Latitude, and it is due not only to the presence of the San Miguel and Agua Blanca faults, but also due to a change in the seismicity of the northern part of the Gulf of California.

One of the initial objectives of this study was to examine the history of strain changes due to earthquakes to see if accumulation in a region during one time interval was followed by release during a subsequent interval. The principal difficulty here is that one does not know the starting conditions. We thus cannot speak of actual strain energy present in a particular locality, but only of changes since some previous time. Only a crude effort can be made in this direction due to the inadequacies of both the model used and the historical data available. By viewing Figures 8 and 9 one can see only a very general relation between areas of net strain energy accumulation during the interval 1812–1915 with areas of net strain release during the subsequent half century. For example we note that the bend in the San Andreas near Fort Tejon causes stress concentration along conjugate planes, one of which extends in the general vicinity of the subsequent Tehachapi earthquakes. The region from Gorman to Cajon Pass shows stress release, and the subsequent history of this region has been remarkably quiet. On the other hand, the stress concentration at the south end of the 1857 break, near Cajon Pass has not yet had any significant effect on seismic activity. To complete the picture, we can also note some regions such as those near the head of the Gulf of California that show a net strain release during both intervals. That this occurs here and in several other localities, is evidence that our model is not entirely adequate, and that other nonseismic types of stress relaxation must be occurring in adjacent regions. Note that the Agua Blanca earthquake of 1892 (No. 3) was inadvertently included in the 1915–1967 interval instead of in the earlier one.

The apparent asymmetry of many of the strain patterns is sometimes the result of a fault being inserted at an angle other than 45° to the assumed principal stress axis, as in the case of the large earthquakes near Santa Barbara and also near San Miguel.

For some of the smaller faults the asymmetry is caused by the superposition of stress field changes from many nearby faults. The discrete approximation used in the numerical integration also causes distortion of the field, particularly for small faults where the mesh points do not fall along the fault in a symmetric fashion. Near the boundaries of the region some distortion can occur; the small band of apparent strain release near the northwest corner of Figure 9 is such an artifact of the computation.

Conclusions

A technique for calculating strain energy changes due to the occurrence of earthquakes has been presented and applied to the southern California, Baja California region. New features of the strain field not discernible in previous strain release maps are brought out. The most important of these is the presence of significant areas of stress concentration resulting from slip on major faults. Limitations of the model used and the historic data available on fault motion prevent a detailed interpretation of the resulting strain maps, however the following tentative conclusions can be drawn:

(1) The 1857 earthquake that ruptured along the bend in the San Andreas near Fort Tejon significantly altered the stress field in this region causing a stress concentration along conjugate planes, one of which lies in the general vicinity of the Tehachapi earthquakes.

(2) Earthquakes in the Santa Barbara area and the Tehachapi area during the past half century have significantly reduced the stored strain energy along the San Andreas in the Fort Tejon vicinity. Thus the probability that a great earthquake can occur here, involving a rupture of the San Andreas through the bend in the fault at Fort Tejon, has been at least temporarily reduced.

(3) A major change in the strain field occurs near 32° north latitude in Baja California. The pattern of strain release confined to a narrow zone along the San Andreas changes here to a broad region transverse to the San Andreas trend.

Acknowledgments

This work was partially supported by National Science Foundation Grant GA 1087 and Air Force Office of Scientific Research Contract AFOSR-62-421. The authors wish to express their thanks to C. F. Richter for his comments and to C. R. Allen and L. E. Alsop for their critical review of the manuscript.

References

Allen, C. R., P. St. Amand, C. F. Richter and J. M. Nordquist (1965). Relationship between seismicity and geologic structure in the southern California region, *Bull. Seism. Soc. Am.* **55**, 753–797.

Benioff, H. (1951). Earthquakes and rock creep, *Bull. Seism. Soc. Am.* **41**, 31–62.

Benioff, H. (1955). Earthquakes in Kern County, California during 1952, *Calif. Dept. of Nat. Resources, Div. Mines, Bull.* **171**, p. 204.

Chinnery, M. A. (1963). The stress changes that accompany strike slip faulting, *Bull. Seism. Soc. Am.* **53**, 593–618.

Fung, Y. C. (1965). *Foundation of Solid Mechanics*, Prentice-Hall, Inc., Englewood Cliffs, New Jersey.

Jeffreys, H. (1962). *The Earth*, Cambridge Univ. Press.

King, Chi-Yu and L. Knopoff (1968). Stress drop in earthquakes, *Bull. Seism. Soc. Am.* **58**, 249–258.

Richter, C. F., and J. M. Nordquist (1951). Instrumental Study of the Manix Earthquakes, *Bull. Seism. Soc. Am.* **41**, 347–388.

Richter, C. F. (1958). *Elementary Seismology*, W. H. Freeman and Company, San Francisco.

Ryall, A., D. Slemmons and L. Gedney (1966). Seismicity, tectonism, and surface faulting in the western United States during historic time, *Bull. Seism. Soc. Am.* **56**, 1105–1136.

Starr, A. T. (1928). Slip in a crystal and rupture in a solid due to shear, *Proc. Camb. Phil. Soc.* **24**, 489–500.

Tsuboi, C. (1952). Earthquake energy, earthquake volume aftershock area, and strength of the Earth's crust, *J. Phys. Earth (Tokyo)* **4**, 63–66.

Wood, H. O. and N. Heck (1951). Earthquake history of the United States. Part II, Stronger earthquakes of California and western Nevada, *U.S. Coast and Geodetic Survey, Ser. No. 609.*

Zienkiewicz, O. and R. Gerstner (1959). A stress function approach to interface and mixed boundary condition problems, *Int. J. Mech. Sci.* **2**, 93–101.

SEISMOLOGICAL LABORATORY
CALIFORNIA INSTITUTE OF TECHNOLOGY
PASADENA, CALIFORNIA (S. W. S.)

LOS ANGELES SCIENTIFIC CENTER
OF INTERNATIONAL BUSINESS
MACHINES CORPORATION
LOS ANGELES, CALIFORNIA (W. V. deL.)

Manuscript received November 22, 1968.

APPENDIX

While most of the numerical technique used is conventional and can be found in any of a number of text books on the subject, the numerical operators used in an interface point may need some explanation.

First the expression in equation (29) is integrated over the area $P_1 P_2 P_3 P_4$. In the case of the boundary going through point P_0 as shown in Figure 11 this gives

$$\int_{S_1+S_2} \nabla^2\phi \, dS = \int_{s_1+s_2} \frac{\partial}{\partial n} \phi \, dl = \int g \, dS = g_1 S_1 + g_2 S_2$$

Using the interface condition (22)

$$g_1 = g_2 + \frac{1}{A} \frac{\partial f_s}{\partial s} .$$

it follows that

$$g_1 = \frac{1}{S_1 + S_2} \int_s \frac{\partial}{\partial n} \phi \, dl + \frac{S_2}{(S_1 + S_2)A} \frac{\partial f_s}{\partial s}$$

$$g_2 = \frac{1}{S_1 + S_2} \int_s \frac{\partial}{\partial n} \phi \, dl - \frac{S_1}{(S_1 + S_2)A} \frac{\partial f_s}{\partial s}$$

These expressions make it possible to calculate g_1 and g_2 when ϕ and $(1/A)(\partial f_s/\partial s)$ are given. As ϕ is continuous [see equation (20)] finite difference approximations can be obtained. The result for g_1 is, for instance

$$g_{i,j}^{(1)} = \frac{1}{(l_1 + l_2)(l_3 + l_4)} \left[\frac{\phi_{i,j+1} - \phi_{i,j}}{2l_1} (l_3 + l_4) + \frac{\phi_{i+1,j} - \phi_{i,j}}{2l_3} (l_1 + l_2) \right.$$

$$\left. + \frac{\phi_{i,j-1} - \phi_{i,j}}{2l_2} (l_3 + l_4) + \frac{\phi_{i-1,j} - \phi_{i,j}}{2l_4} (l_1 + l_2)\{l_2 \, l_3\} \frac{1}{A} \frac{\partial f_s}{\partial s} \right]$$

A similar expression for $g_{i,j}^{(2)}$ can be found.

The ϕ used in these expressions are not correct yet and consequently the g's calculated do not satisfy equation (28) but rather

$$\nabla^2 g = r$$

The quantity r is used in the iteration to correct g. A finite difference approximation has to be made of this equation. For the regular grid points this is conventional, however for points lying on an interface the expression will be derived here for the interface going through the point as shown in Figure 11.

Again integrating equation (28) over $P_1 P_2 P_3 P_4$ gives

$$\int_S \nabla^2 g \, dS = \int \frac{\partial}{\partial n} g \, dl = \int r \, dS$$

In writing down the finite difference form of the line integral on the right hand side it should be kept in mind that g is two-valued on the interface.

$$\int r dS = (g_{i,j+1} - g^{(1)}_{i,j}) \frac{l_3 + l_4}{2l_1} + (g_{i-1,j} - g^{(1)}_{i,j}) \frac{l_1 + l_2}{2l_4} + (g^{(1)}_{i,j-1} - g^{(1)}_{i,j}) \frac{l_4}{2l_2} +$$

$$(g^{(2)}_{i,j-1} - g^{(2)}_{i,j}) \frac{l_3}{2l_2} + (g^{(1)}_{i+1,j} - g^{(1)}_{i,j}) \frac{l_1}{2l_3} + (g^{(2)}_{i+1,j} - g^{(2)}_{i,j}) \frac{l_2}{2l_3} = R_{i,j}$$

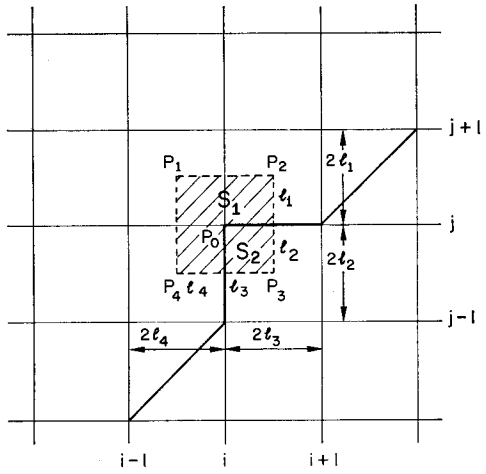

FIG. 11. Illustration of interface operator for use in the discrete representation of a curved fault.

When using point interation, $g^{(1)}_{i,j}$ and $g^{(2)}_{i,j}$ are to be corrected to a value that makes this expression equal to zero. First $g^{(2)}$ is replaced by

$$g^{(2)}_{i,j} = g^{(1)}_{i,j} - \frac{1}{A} \left(\frac{\partial f_s}{\partial s} \right)_{i,j}$$

after which it is possible to calculate the necessary change in $g^{(1)}_{i,j}$. If the k^{th} iterate is known, the $(k+1)^{\text{th}}$ iterate can be found from

$$^{(k+1)}g^{(1)}_{i,j} = {}^{(k)}g^{(1)}_{i,j} + \epsilon^{(k)}_{i,j} \tag{30}$$

where

$$\varepsilon^{(k)}_{i,j} = R_{i,j} \Big/ \left(\frac{l_3 + l_4}{2l_1} + \frac{l_3 + l_4}{2l_2} + \frac{l_1 + l_2}{2l_3} + \frac{l_1 + l_2}{2l_4} \right)$$

If over or under relaxation is used equation (30) is changed to

$$^{(k+1)}g^{(1)}_{i,j} = {}^{(k)}g^{(1)}_{i,j} + \omega\epsilon^{(k)}_{i,j}$$

where ω is the relaxation factor.
The new $^{(k+1)}g^{(2)}_{i,j}$ is obtained from:

$$^{(k+1)}\, g^{(2)}_{i,j} = {}^{(k+1)}g^{(1)}_{i,j} - \frac{1}{A}\left(\frac{\partial f_s}{\partial s}\right)_{i,j}$$

Similar expressions hold for points in which the interface has another shape.

For regular points the same expressions are valid, however the quantity $(1/A)(\partial f_s/\partial s)$ is equal to zero in those points, making $g^{(1)} = g^{(2)}$.